Supporting Information

Di-nuclear platinum complexes containing aryl-isoquinoline and oxadiazole-thiol with an efficiency over 8.8%: In-depth investigation on relationship between the molecular structure and near-infrared electroluminescent properties in PLEDs

Wenjing Xiong,[a] Fanyuan Meng,[a,c] Hua Tan,[a] Pu Wang,[a] Youming Zhang,[a] Qiang Tao,[a] Yu Liu,[a] Shijian Su,[c]* Weiguo Zhu,[a, b]**

Contents

Figure S1. Representative frontier orbitals for $(piq)_2Pt_2(\mu\text{-PhOXT})_2$.

Figure S2. Representative frontier orbitals for $(piq)_2Pt_2(\mu\text{-}C_8OXT)_2$.

Figure S3. Representative frontier orbitals for $(2niq)_2Pt_2(\mu\text{-}C_8OXT)_2$.

Figure S4. PL spectra of the dinuclear platinum complexes in DCM (10^{-5} M) at 77 K.

Figure S5. Optimal structure of $(piq)_2Pt_2(\mu\text{-PhOXT})_2$ (a), $(piq)_2Pt_2(\mu\text{-}C_8PhOXT)_2$ (b) and $(2niq)_2Pt_2(\mu\text{-}C_8PhOXT)_2$ (c). Selected dihedral angles: (a) N11-C36-C35-C26: 10.28°, N12-C60-C61-C51: 11.52°; (b) N2-C3-C11-C12: 10.33°, N44-C45-C53-C54: 13.28°; (c) N2-C3-C11-C12: 20.12°, N44-C45-C53- C54: 20.41°.

Figure S6. EL spectra of the $(piq)_2Pt_2(\mu\text{-PhOXT})_2$-, $(piq)_2Pt_2$ -$(\mu\text{-}C_8PhOXT)_2$- and $(2niq)_2Pt_2(\mu\text{-}C_8PhOXT)_2$-doped devices at different dopant concentrations from 6 wt% and 9 wt% to 12 wt%.

Figure S7. The *J-V-R* curves of the the $(piq)_2Pt_2(\mu\text{-PhOXT})_2$-, $(piq)_2Pt_2(\mu\text{-}C_8Ph$ $OXT)_2$- and $(2niq)_2Pt_2(\mu\text{-}C_8PhOXT)_2$-doped devices at different dopant concentrations from 6 wt% and 9 wt% to 12 wt%.

Figure S8. *EQE-J* curves of the $(piq)_2Pt_2(\mu\text{-PhOXT})_2$-, $(piq)_2Pt_2$ $(\mu\text{-}C_8PhOXT)_2$- and $(2niq)_2Pt_2(\mu\text{-}C_8PhOXT)_2$-doped devices at different dopant concentrations from 6 wt% and 9 wt% to 12 wt%.

Figure S9. ^1H NMR of $(piq)_2Pt_2(\mu\text{-PhOXT})_2$ (a) , $(piq)_2Pt_2(\mu\text{-}C_8PhOXT)_2$ (b) and $(2niq)_2Pt_2(\mu\text{-}C_8PhOXT)_2$ (c).

Figure S10. ^{13}C NMR of $(piq)_2Pt_2(\mu\text{-PhOXT})_2$ (a), $(piq)_2Pt_2(\mu\text{-}C_8PhOXT)_2$ (b) and

$(2niq)_2Pt_2(\mu\text{-}C_8PhOXT)_2$ (c).

Figure S11. MALDI-TOF MS plots of $(piq)_2Pt_2(\mu\text{-}PhOXT)_2$ (a), $(piq)_2Pt_2(\mu\text{-}C_8Ph\text{-}OXT)_2$ (b) and $(2niq)_2Pt_2(\mu\text{-}C_8PhOXT)_2$ (c)

Table S1. Calculated excitation energy (E), oscillator strength (f), dominant contributing transitions and associated percent contribution and assignment of complexes $(piq)_2Pt_2(\mu\text{-}PhOXT)_2$, $(piq)_2Pt_2(\mu\text{-}C_8OXT)_2$ and $(2niq)_2Pt_2(\mu\text{-}C_8OXT)_2$ (c).

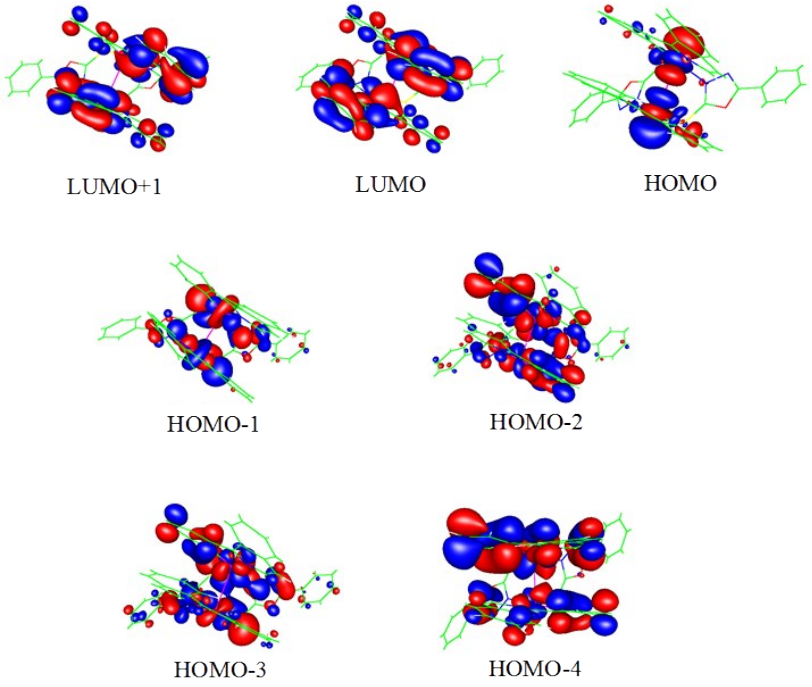

Figure S1. Representative frontier orbitals for $(piq)_2Pt_2(\mu\text{-}PhOXT)_2$.

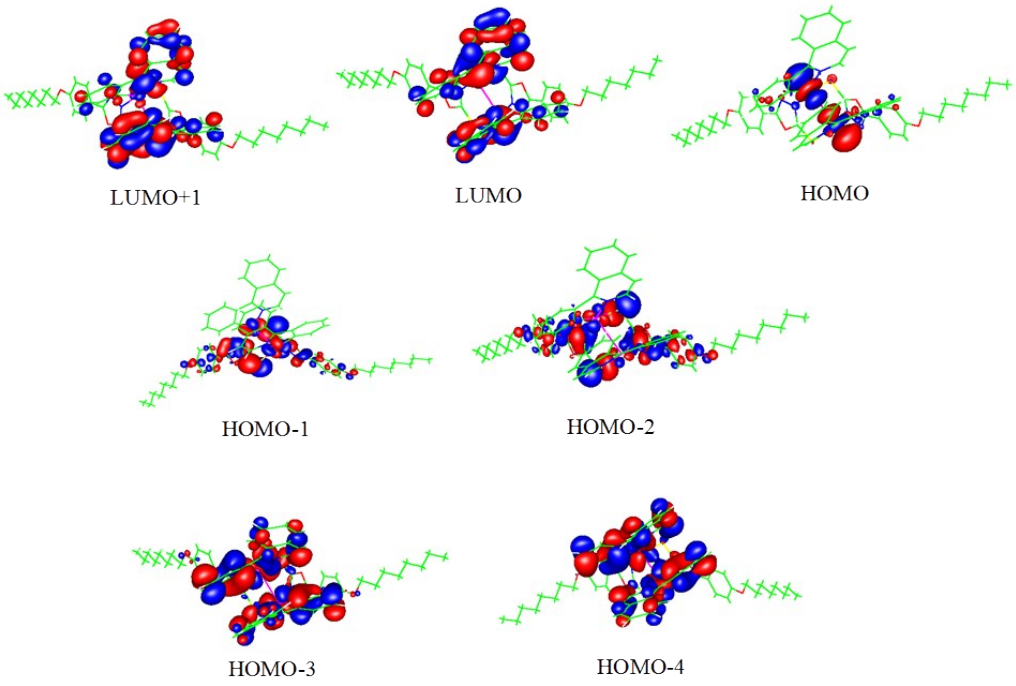

Figure S2. Representative frontier orbitals for $(piq)_2Pt_2(\mu\text{-}C_8OXT)_2$.

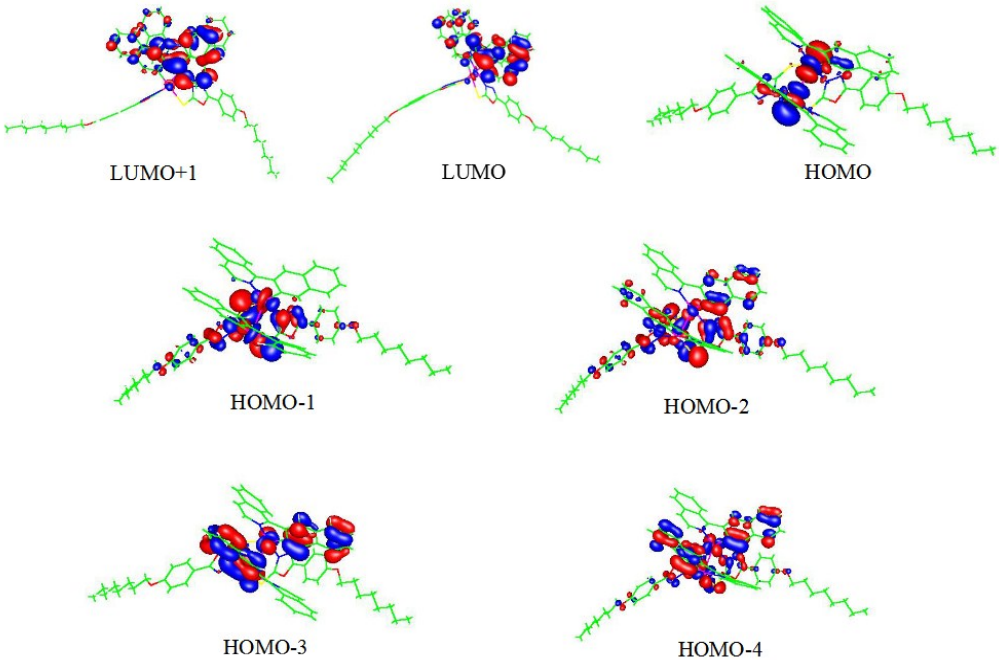

Figure S3. Representative frontier orbitals for $(2niq)_2Pt_2(\mu\text{-}C_8OXT)_2$.

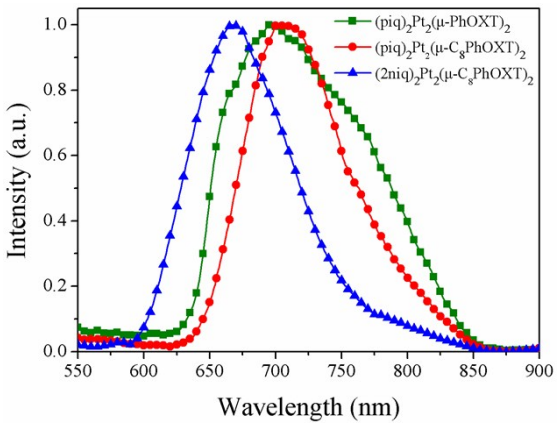

Figure S4. PL spectra of the dinuclear platinum complexes in DCM (10^{-5} M) at 77 K.

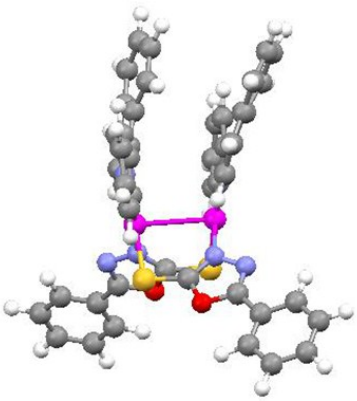

(a)

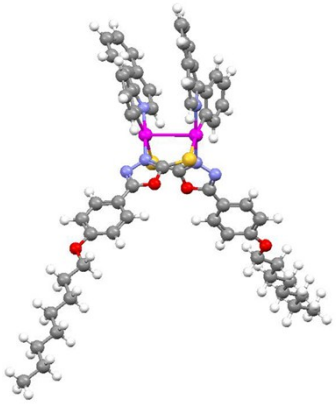

(b)

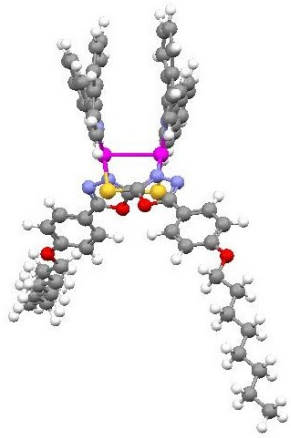

(c)

Figure S5. Optimal structure of $(piq)_2Pt_2(\mu\text{-PhOXT})_2$ (a), $(piq)_2Pt_2(\mu\text{-C}_8\text{PhOXT})_2$ (b) and $(2niq)_2Pt_2(\mu\text{-C}_8\text{PhOXT})_2$ (c). Selected dihedral angles: (a) N11-C36-C35-C26: 10.28°, N12-C60-C61-C51: 11.52°; (b) N2-C3-C11-C12: 10.33°, N44-C45-C53-C54: 13.28°; (c) N2-C3-C11-C12: 20.12°, N44-C45-C53- C54: 20.41°.

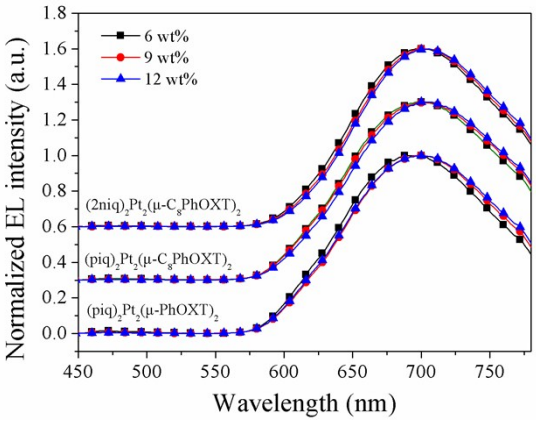

Figure S6. EL spectra of the $(piq)_2Pt_2(\mu\text{-PhOXT})_2$-, $(piq)_2Pt_2(\mu\text{-C}_8\text{PhOXT})_2$- and $(2niq)_2Pt_2(\mu\text{-C}_8\text{PhOXT})_2$-doped devices at different dopant concentrations from 6 wt% and 9 wt% to 12 wt%.

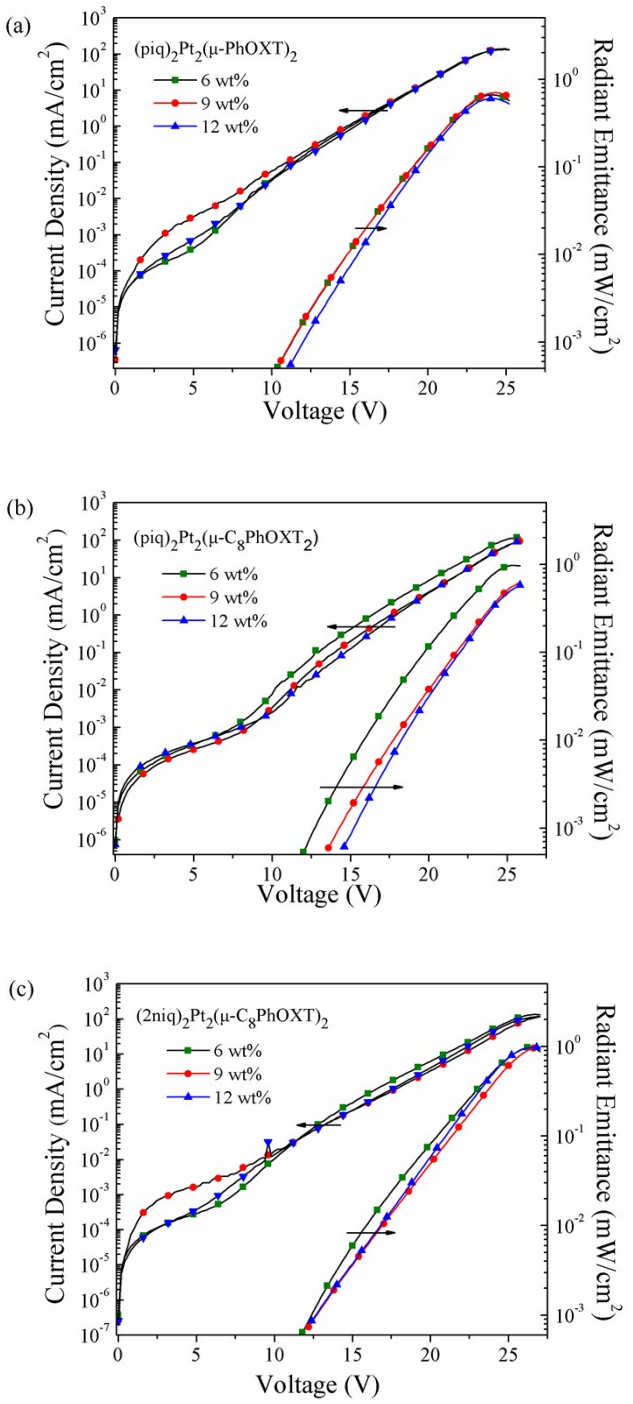

Figure S7. The *J-V-R* curves of the the $(piq)_2Pt_2(\mu\text{-PhOXT})_2$-, $(piq)_2Pt_2(\mu\text{-C}_8\text{PhOXT})_2$- and $(2niq)_2Pt_2(\mu\text{-C}_8\text{PhOXT})_2$-doped devices at different dopant concentration -s from 6 wt% and 9 wt% to 12 wt%.

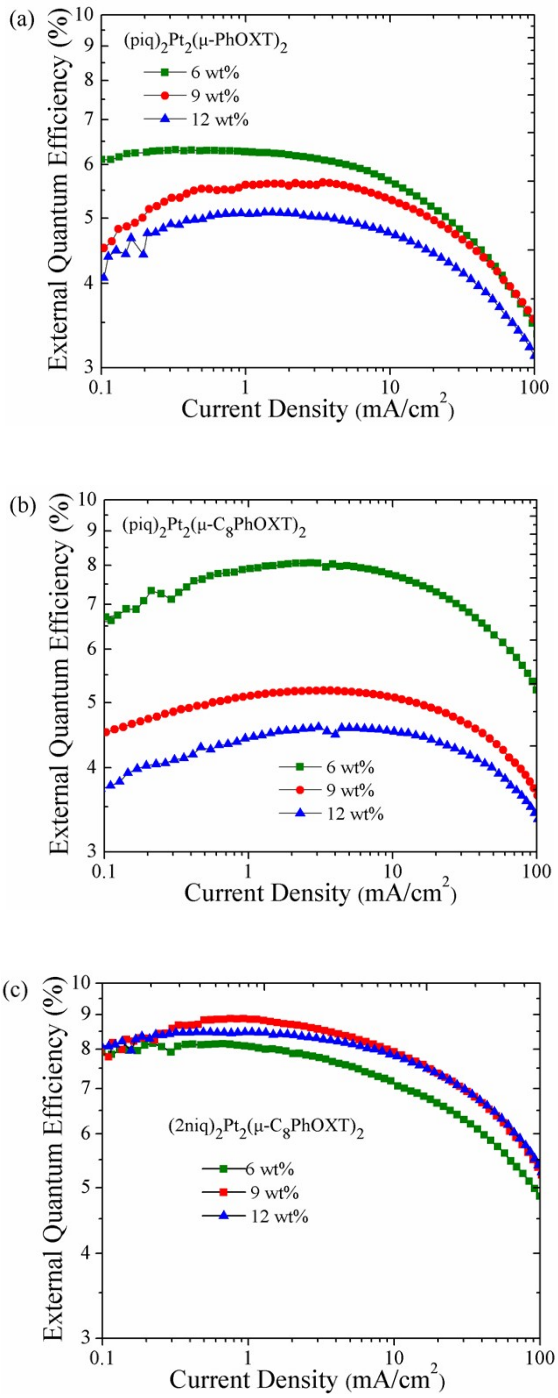

Figure S8. *EQE-J* curves of the $(piq)_2Pt_2(\mu\text{-PhOXT})_2$-, $(piq)_2Pt_2(\mu\text{-C}_8\text{PhOXT})_2$- and $(2niq)_2Pt_2(\mu\text{-C}_8\text{PhOXT})_2$-doped devices at different dopant concentrations from 6 wt% and 9 wt% to 12 wt%.

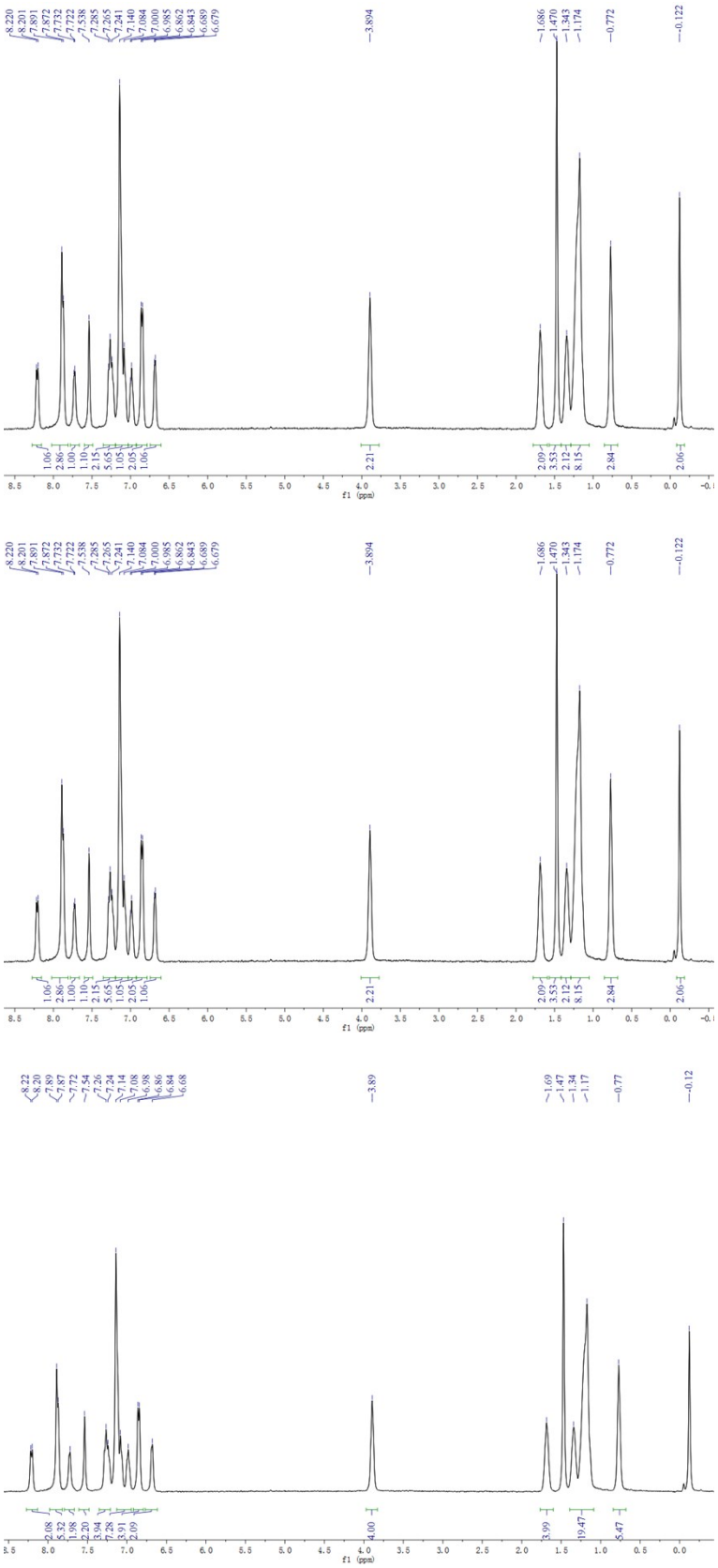

Figure S9. ^{1}H NMR of $(piq)_2Pt_2(\mu\text{-PhOXT})_2$ (a) , $(piq)_2Pt_2(\mu\text{-C}_8\text{PhOXT})_2$ (b) and $(2niq)_2Pt_2(\mu\text{-C}_8\text{PhOXT})_2$ (c).

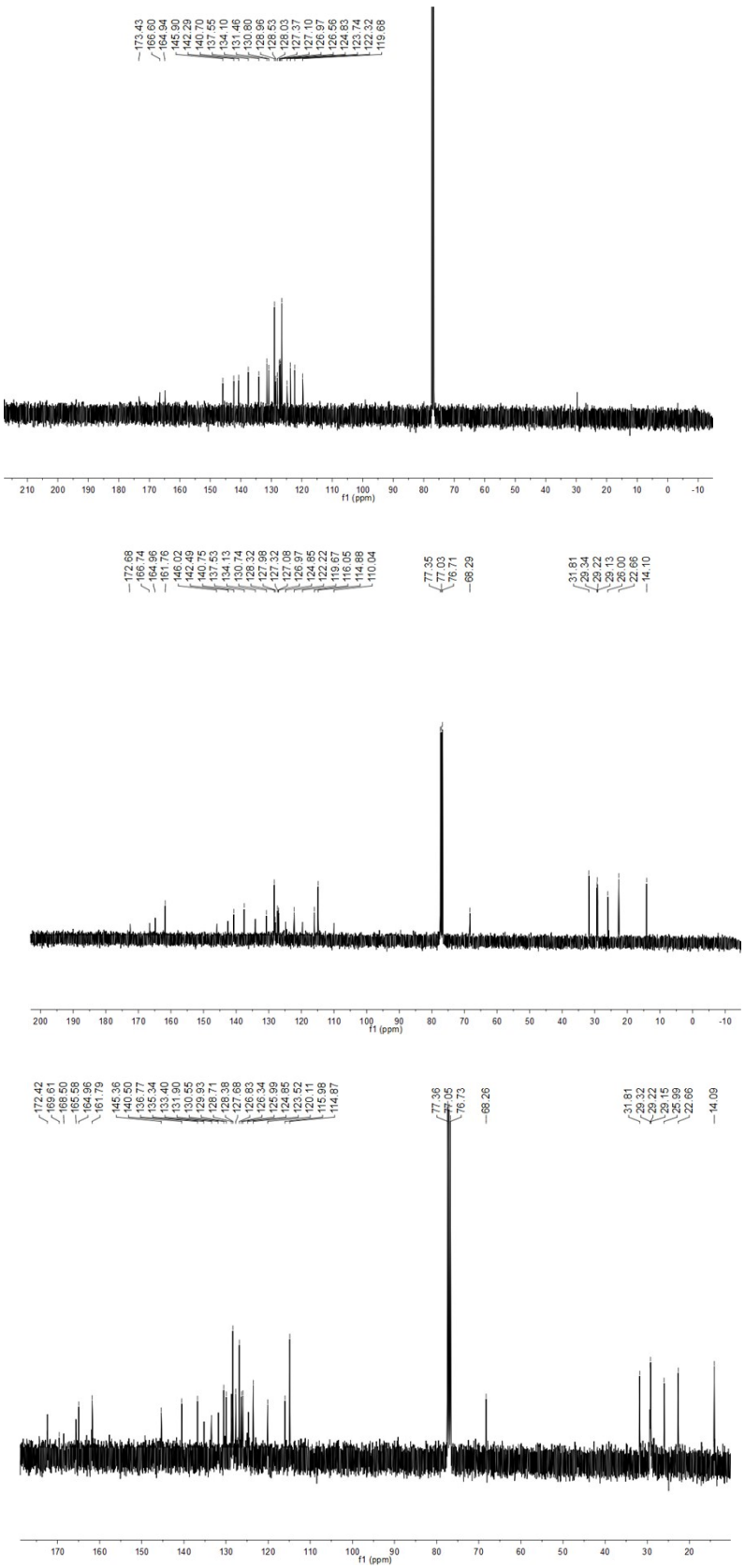

Figure S10. ^{13}C NMR of $(piq)_2Pt_2(\mu\text{-PhOXT})_2$ (a), $(piq)_2Pt_2(\mu\text{-C}_8\text{PhOXT})_2$ (b) and $(2niq)_2Pt_2(\mu\text{-C}_8\text{PhOXT})_2$ (c).

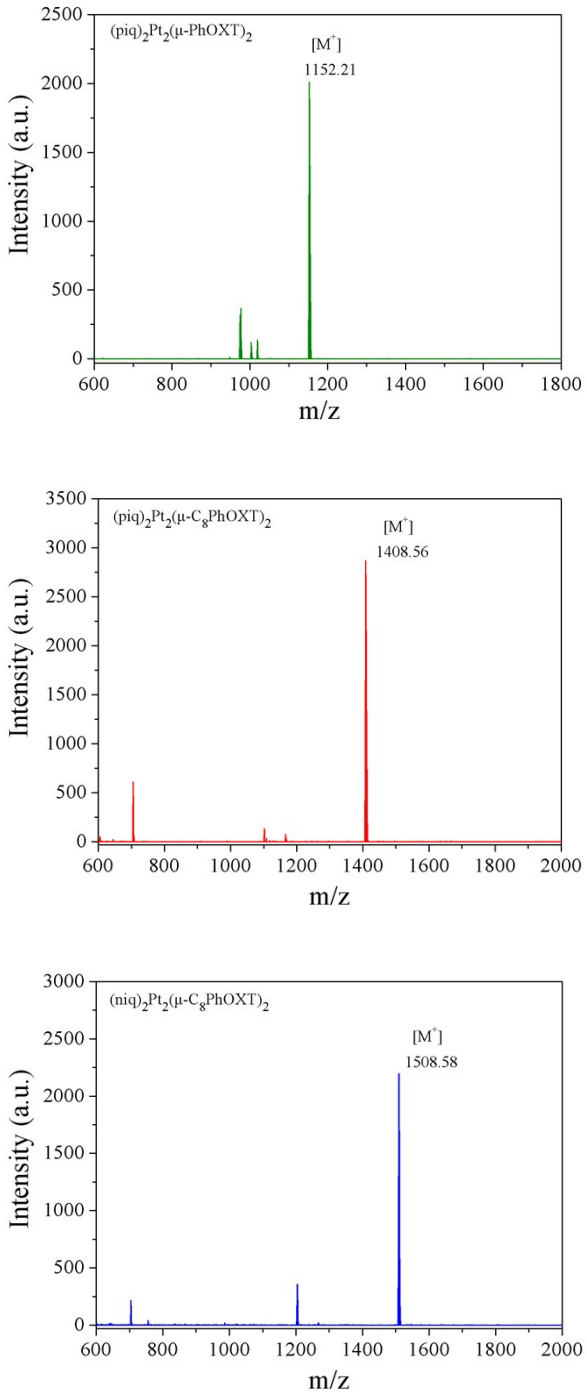

Figure S11. MALDI-TOF MS plots of $(piq)_2Pt_2(\mu\text{-PhOXT})_2$ (a), $(piq)_2Pt_2(\mu\text{-C}_8\text{PhOXT})_2$ (b) and $(2niq)_2Pt_2(\mu\text{-C}_8\text{PhOXT})_2$ (c).

Table S1. Calculated excitation energy (E), oscillator strength (f), dominant contributing transitions and associated percent contribution and assignment of complexes $(piq)_2Pt_2(\mu\text{-PhOXT})_2$, $(piq)_2Pt_2(\mu\text{-}C_8OXT)_2$ and $(2niq)_2Pt_2(\mu\text{-}C_8OXT)_2$ (c).[a]

complex	S_n	E/eV	E/nm	f	dominant transitions (percent contribution[b])	assignment
$(piq)_2Pt_2(\mu\text{-PhOXT})_2$	1	2.64	469.7	0.018	HOMO → LOMO (98.8%)	MMLCT
	2	2.93	423.2	0.006	HOMO → LOMO+1 (98.2%)	MMLCT
	3	2.99	414.7	0.002	HOMO –1 → LOMO (98.4%)	MLLCT
	4	3.25	381.5	0.013	HOMO –2 → LOMO (71.9%)	LLCT
					HOMO –3 → LOMO (24.3%)	
	5	3.28	378.0	0.007	HOMO –1 → LOMO+1 (90.7%)	LLCT
	6	3.06	405.2	0.011	HOMO –2 → LOMO (21.4%)	LLCT
					HOMO –3 → LOMO (71.7%)	
	7	3.22	385.1	0.035	HOMO –4 → LOMO (15.7%)	ILCT
					HOMO –2 → LOMO+1 (66.8%)	ILCT
					HOMO –2 → LOMO+1 (66.8%)	ILCT
	8	3.54	350.3	0.005	HOMO –4 → LOMO (15.7%)	ILCT
					HOMO –3 → LOMO+1 (15.0%)	LLCT
$(piq)_2Pt_2(\mu\text{-}C_8OXT)_2$	1	2.63	471.5	0.025	HOMO → LOMO (98.8%)	MMLCT
	2	2.83	438.2	0.008	HOMO → LOMO+1 (97.9%)	MMLCT
	3	2.85	435.1	0.001	HOMO –1 → LOMO (98.1%)	MLLCT
	4	2.98	416.1	0.011	HOMO –2 → LOMO (89.2%)	LLCT
					HOMO –3 → LOMO (6.3%)	ILCT
	5	3.05	406.6	0.003	HOMO –1 → LOMO+1 (95.7%)	LLCT
	6	3.18	389.9	0.007	HOMO –2 → LOMO+1 (85.7%)	LLCT
					HOMO –3 → LOMO+1 (6.2%)	ILCT
	7	3.32	373.5	0.008	HOMO –3 → LOMO (87.0%)	ILCT
					HOMO –2 → LOMO (6.8%)	LLCT
	8	3.42	362.6	0.034	HOMO –4 → LOMO (82.7%)	ILCT
					HOMO –2 → LOMO+1 (7.2%)	LLCT
					HOMO –3 → LOMO+1 (4.8%)	ILCT
	9	3.29	376.9	0.009	HOMO –4 → LOMO (84.4%)	ILCT
					HOMO –3 → LOMO+1 (9.3%)	
	10	3.62	342.5	0.021	HOMO –4 → LOMO+1 (82.7%)	ILCT
$(2niq)_2Pt_2(\mu\text{-}C_8OXT)_2$	1	2.46	504.1	0.068	HOMO → LOMO (98.5%)	MMLCT
	2	2.65	467.9	0.076	HOMO → LOMO+1 (97.7%)	MMLCT
	3	2.75	450.9	0.082	HOMO –1 → LOMO (96.8%)	MLLCT
	4	2.72	455.9	0.086	HOMO –2 → LOMO (47.5%)	LLCT
					HOMO –3→ LOMO (42.2%)	LLCT
					HOMO –2 → LOMO+1 (3.4%)	LLCT
	5	2.77	477.7	0.089	HOMO –1 → LOMO+1 (65.7%)	LLCT
					HOMO –2 → LOMO (17.2%)	LLCT
					HOMO –3→ LOMO (11.5%)	LLCT

				HOMO –3→ LOMO (35.0%)	LLCT
6	2.67	464.4	0.090	HOMO –1 → LOMO+1 (31.2%)	LLCT
				HOMO –2 → LOMO (19.1%)	LLCT
				HOMO –4 → LOMO (5.1%)	ILCT
				HOMO –2 → LOMO+1 (40.1%)	LLCT
7	2.87	432.1	0.093	HOMO –3 → LOMO+1 (27.0%)	LLCT
				HOMO –2 → LOMO (13.1%)	LLCT
				HOMO –4 → LOMO (12.6%)	LLCT
				HOMO –2 → LOMO+1 (49.8%)	LLCT
8	2.88	430.6	0.097	HOMO –3 → LOMO+1 (32.7%)	LLCT
				HOMO –4 → LOMO (9.9%)	LLCT
9	3.01	412.0	0.098	HOMO –4 → LOMO (66.0%)	LLCT
				HOMO –3 → LOMO+1 (29.7%)	LLCT

[a] Computed at the DFT/B3LYP/def-tzvp. [b] The actual percent contribution = (configuration coefficient)$^2 \times 2 \times 100\%$.